

CHEMISTRY

A European Journal



Accepted Article

Title: Gadolinium(III)-based Dual $^1\text{H}/^{19}\text{F}$ MRI Probes

Authors: Rosa Pujales-Paradela, Tanja Savić, David Esteban-Gomez, Goran Angelovski, Fabio Carniato, Mauro Botta, and C. Platas-Iglesias

This manuscript has been accepted after peer review and appears as an Accepted Article online prior to editing, proofing, and formal publication of the final Version of Record (VoR). This work is currently citable by using the Digital Object Identifier (DOI) given below. The VoR will be published online in Early View as soon as possible and may be different to this Accepted Article as a result of editing. Readers should obtain the VoR from the journal website shown below when it is published to ensure accuracy of information. The authors are responsible for the content of this Accepted Article.

To be cited as: *Chem. Eur. J.* 10.1002/chem.201806192

Link to VoR: <http://dx.doi.org/10.1002/chem.201806192>

Supported by
ACES

WILEY-VCH

Gadolinium(III)-based Dual $^1\text{H}/^{19}\text{F}$ MRI Probes

Rosa Pujales-Paradela,^[a] Tanja Savić,^[b] David Esteban-Gómez,^[a] Goran Angelovski,^{*,[b]} Fabio Carniato,^[c] Mauro Botta,^{*,[c]} Carlos Platas-Iglesias^{*,[a]}

Abstract: We present two novel octadentate cyclen-based ligands containing one (L^1) or two (L^2) phenylacetamide pendants that feature two CF_3 groups either at positions 3 and 5 (L^1) or 4 (L^2). The corresponding Gd^{3+} complexes possess one coordinated water molecule, as confirmed by the luminescence lifetime measurements recorded on the Eu(III) and Tb(III) analogues. A detailed ^1H and ^{17}O relaxometric characterisation revealed the parameters that govern the relaxivities of these complexes. The water exchange rate of the mono-amide derivative GdL^1 ($k_{\text{ex}}^{298} = 1.52 \times 10^6 \text{ s}^{-1}$) is faster than that determined for the bis-amide complex GdL^2 ($k_{\text{ex}}^{298} = 0.73 \times 10^6 \text{ s}^{-1}$). ^1H and ^{19}F NMR studies indicate that the complexes are present in solution almost exclusively as the square antiprismatic (SAP) isomers. ^{19}F NMR relaxation studies provided $\text{Gd}\cdots\text{F}$ distances of 7.4 ± 0.1 and $9.1 \pm 0.1 \text{ \AA}$ for GdL^1 and GdL^2 , respectively. Phantom MRI studies revealed the favourable properties of GdL^2 as a dual $^1\text{H}/^{19}\text{F}$ MRI probe, while the shorter $\text{Gd}\cdots\text{F}$ distance of GdL^1 reduces the signal to noise ratio due to the very short transverse relaxation time of the ^{19}F NMR signal.

Introduction

Magnetic resonance imaging (MRI) is a non-invasive technique that uses nuclear magnetic resonance principles for generating 3D-anatomical images with very high resolution and unlimited depth penetration.^[1] MRI images are based on the alignment of nuclear spins to an external magnetic field, which can be perturbed by applying a radiofrequency pulse. The nuclear spins then return to the initial state at different rates after the application of the pulse (relaxation). Contrast in MRI can be achieved by taking advantage of the differences in relaxation times of water proton nuclei of different tissues. However, image contrast can be improved by manipulating the relaxation times with the so called contrast agents (CAs).^[1-3] These substances are designed to improve the sensitivity and quality of the images, usually producing brighter images by shortening the longitudinal relaxation times of water protons (T_1 -weighted

agents). CAs are usually paramagnetic metal complexes, generally containing the lanthanide ion Gd^{3+} . Gadolinium contrast agents (GdCAs) affect the longitudinal (T_1) and transverse (T_2) relaxation times of water proton nuclei, shortening both components. The choice of Gd^{3+} is related to its electronic properties (seven unpaired electrons, high effective magnetic moment at room temperature - $\mu^2 = 63 \text{ BM}^2$ - and a long relaxation time of the electron spin).^[4]

The most robust CAs used in clinical practice are macrocyclic Gd^{3+} complexes such as $[\text{Gd}(\text{DOTA})]^-$ (DOTAREM[®]), as the macrocyclic ligand ensures a high stability and inertness with respect to complex dissociation.^[5] Indeed, some toxicity problems have been attributed to the dissociation of GdCAs, most often after administration of non-macrocyclic derivatives.^[6] As a consequence of these toxicity issues, restrictions and suspensions of authorisations of some of the linear GdCAs have been executed recently by the European Medicines Agency.^[7] These restrictions do not affect macrocyclic agents, which are kinetically more inert than the linear ones.^[8] Another disadvantage of traditional T_1 CAs is the presence of a background signal due to the bulk water. In the last decades, different alternatives were explored to improve the sensitivity and reduce the toxicity and acquisition times of the MRI scans.^[9] Among several of the targets set for these improvements are, for instance, the use of other metal ions (i.e. Mn^{2+} ,^[10] Fe^{3+} ,^[11] Fe^{2+} ,^[12] Co^{2+} ,^[13] Ni^{2+} ^[14]) potentially less harmful than gadolinium in case of release, the development of new modalities of imaging (i.e. paraCEST,^[12-16] paraSHIFT,^[17] responsive or smart agents^[18,19]) or the use of diverse approaches combined on the same probe (i.e. multimodal or multiresponsive probes).^[20]

Fluorinated probes are one of the most attractive approaches to overcome the issue associated with the background signal of bulk water.^[21,22] Some of the reasons that make these systems quite promising are that fluorinated substances are almost absent in the human body, being present only in teeth and bones as solid salts.^[23] Thus, one can obtain images at the frequency of ^{19}F without the background due to this nucleus. This solves the water-background signal problem, improving the signal-to-noise ratio (SNR) on the recorded images. Other properties that make attractive this nucleus is the high gyromagnetic ratio (40.05 MHz/T), its isotopic abundance ratio (100%), its non-quadrupolar nature ($I = \frac{1}{2}$) and wide chemical shift range (~350 ppm), and the similar sensitivity to ^1H (83%). Another noteworthy feature is the possibility of using the same scanners than for standard ^1H MRI, with just small adjustments on the Larmor frequency for detecting the ^{19}F nuclei (i.e. tuning at 282 MHz for ^{19}F instead of 300 MHz for ^1H). Fluorinated compounds have relatively long relaxation rates, and consequently acquisition times would be rather long.^[23, 24] This issue can be solved by introducing a paramagnetic centre, either a transition metal^[24,25] or lanthanide metal ions,^[23,26-29] in the vicinity of ^{19}F nuclei, which shortens both T_1 and T_2 relaxation

[a] R. Pujales-Paradela, Dr. D. Esteban-Gómez, Dr. C. Platas-Iglesias
Centro de Investigaciones Científicas Avanzadas (CICA) and
Departamento de Química, Facultad de Ciencias, Universidade da
Coruña, 15071 A Coruña, Galicia, Spain
Email: carlos.platas.iglesias@udc.es

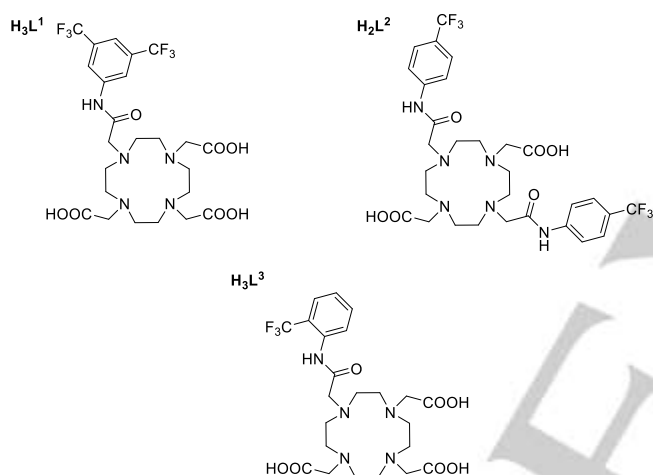
[b] T. Savić, Dr. G. Angelovski
MR Neuroimaging Agents, Max Planck Institute for Biological
Cybernetics, Tuebingen, Germany
Email: goran.angelovski@tuebingen.mpg.de

[c] F. Carniato, Prof. M. Botta
Dipartimento di Scienze e Innovazione Tecnologica, Università del
Piemonte Orientale "A. Avogadro", Viale T. Michel 11, 15121
Alessandria, Italy
Email: mauro.botta@uniupo.it

Supporting information for this article is given via a link at the end of the document.

times through the paramagnetic relaxation enhancement (PRE) effect.^[22,27c] While the shortening the longitudinal relaxation times leads to a decrease on the acquisition times, reducing T_2 causes line-broadening, and thus decreases signal intensity, sensitivity and the final resolution of the collected images. Hence, optimal probes should present a T_2/T_1 ratio close to the unit.^[30]

The ^{19}F probes based on Ln^{3+} ions so far investigated were designed for the paramagnetic ions of the second part of the lanthanide series (Tb^{3+} to Yb^{3+}). These Ln^{3+} ions combine a high effective magnetic moment and relatively long relaxation times of the electron spin, which prevents extensive line-broadening.^[31] The detailed work of Parker and co-workers concluded that for these metal ions the optimal distance between the paramagnetic ion and the ^{19}F nuclei should be in the range 5-7 Å.^[26] A typical scaffold used by Parker et al. to achieve this range of $\text{Ln}\cdots\text{F}$ distances is represented by ligand H_3L^3 (Scheme 1).



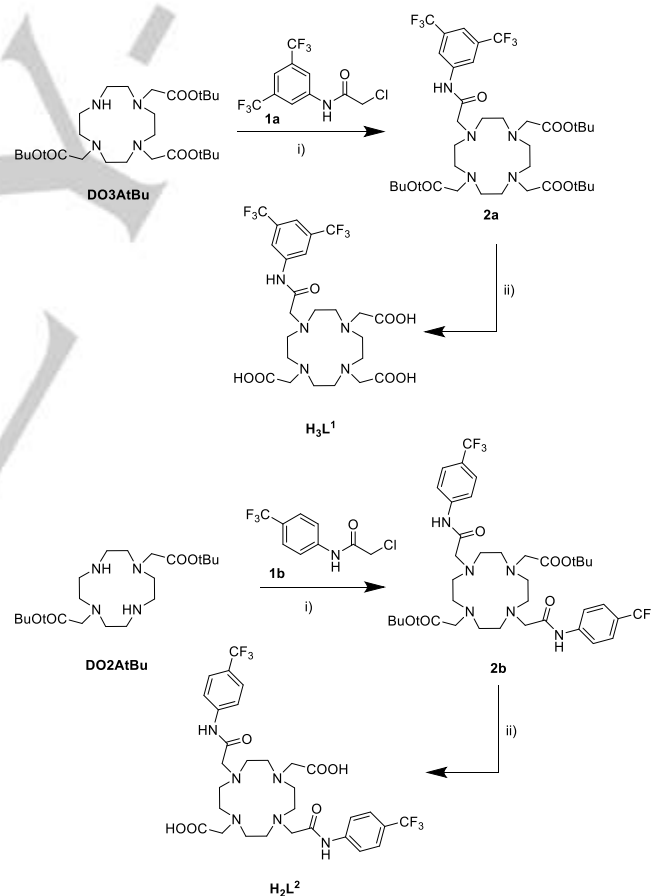
Scheme 1. Chemical structure of the ligands studied in this work.

We hypothesised that a careful selection of the distance between the paramagnetic Gd^{3+} ion and the ^{19}F nuclei would allow the preparation of genuine dual Gd^{3+} -based $^1\text{H}/^{19}\text{F}$ probes. These agents would combine the robustness and sensitivity of traditional T_1 agents with the background-free images provided by ^{19}F , which should allow for quantification of the probe concentration. Thus, herein we report the synthesis of the cyclen-based ligands H_3L^1 and H_2L^2 (Scheme 1), which contain two CF_3 groups at different positions of the phenylacetamide pendant arms. This allows for a comparison of the effect of the $\text{Gd}\cdots\text{F}$ distance on the ^{19}F relaxation times. Furthermore, we present a complete relaxometric study including proton nuclear magnetic relaxation dispersion (^1H NMRD) profiles and ^{17}O and ^{19}F chemical shifts and relaxation measurements. In addition, we report a structural study of the Gd^{3+} complexes in solution using DFT calculations in combination with the analysis of the ^1H NMR spectra of the Eu^{3+} analogue and luminescence lifetimes of the Eu^{3+} and Tb^{3+} derivatives. Finally, we also report *in vitro* MRI studies on tube phantoms at both the ^1H and ^{19}F frequencies.

Results and Discussion

Synthesis. The synthesis of ligands H_3L^1 and H_2L^2 was undertaken by an alkylation of the tris- or bis-protected cyclen derivatives DO3AtBu or DO2AtBu , respectively, with chloromethyl acetamides **1a** and **1b** (Scheme 2). These precursors were prepared in one step by reaction of chloroacetyl chloride with the respective fluorinated aniline.^[32,33] The ligands were isolated with nearly quantitative overall yields (> 98%) upon cleavage of the *tert*-butyl protecting groups with formic acid.

The preparation of the complexes was undertaken by using a solvothermal method, employing hydrated LnCl_3 ($\text{Ln} = \text{Eu}, \text{Gd}$ or Tb), *n*-butanol as solvent and DIPEA as a base. The complexation of Ln^{3+} ions by macrocyclic ligands is known to be faster in non-aqueous media.^[34] The purification of the complexes was achieved by reverse-phase medium performance liquid chromatography (MPLC). The high-resolution mass spectra (Figures S1-S6, Supporting Information) confirm the formation of the complexes.



Scheme 2. Synthesis of the ligands reported in this work. Reagents and conditions: i) CH_3CN , K_2CO_3 , 45 °C, 9 days; ii) HCOOH , 80 °C, 48 h.

r_{1p} determination and hydration numbers. The relaxation enhancement of water protons induced by the presence of a

paramagnetic agent at 1 mM concentration, known as relaxivity (r_{1p}), represents a straightforward measure of the efficiency of a paramagnetic complex as a T_1 -weighted contrast agent *in vitro*.^[35] The relaxivities of both gadolinium complexes were measured at 298 K and 300 MHz from aqueous solutions buffered at pH 7.4 (0.05 M HEPES). The measured paramagnetic relaxation enhancements present a linear dependence with Gd^{3+} concentration (measured using 2.5-4.5 mM solutions). The slopes of the straight lines (Figure S7, Supporting Information) provide the relaxivities of the complexes, resulting in values $r_{1p} = 4.85 \text{ mM}^{-1} \text{ s}^{-1}$ and $3.97 \text{ mM}^{-1} \text{ s}^{-1}$ for GdL^1 and GdL^2 , respectively. These relaxivity values are respectively similar to those of monohydrated neutral and positively charged complexes with similar size, indicating the presence of one water molecule coordinated to the metal ion ($q=1$) in both systems.^[36]

Table 1. Emission lifetimes and hydration numbers obtained for the complexes of L^1 and L^2 .

	$\tau(\text{H}_2\text{O})$ [ms]	$\tau(\text{D}_2\text{O})$ [ms]	$q^{[a]}$
EuL^1	0.607	1.85	1.0
TbL^1	1.85	3.10	0.8
EuL^2	0.663	1.59	0.6
TbL^2	1.71	2.92	0.9

[a] Obtained using the method proposed by Beeby, ref. [37].

The hydration numbers of the GdL^1 and GdL^2 complexes were further investigated by measuring the emission lifetimes of the excited 5D_0 of the Eu^{3+} and the 5D_4 of the Tb^{3+} analogues in solutions of the complexes in H_2O and D_2O (Table 1).^[37] The lifetimes of both the Eu^{3+} and Tb^{3+} complexes are typical of mono-hydrated complexes,^[38] and the hydration numbers calculated using the methodology proposed by Beeby^[37] confirms the formation of $q = 1$ complexes.

Solution structure. The ^1H NMR spectra of the EuL^1 and EuL^2 complexes are rather well resolved, presenting paramagnetically shifted signals in the range ~ -20 -35 ppm (Figure 1). The signals of the most shifted axial protons of the macrocyclic unit are observed in the range 27-34 ppm, which is typical of DOTA-like complexes adopting square antiprismatic geometries in solution.^[39] The presence of a broad signal at ~ 10 -12 ppm likely reflects the presence of a small amount of the twisted-square antiprismatic isomer. The spectra of the two complexes are very similar, indicating that they present very similar structures in solution. The corresponding ^{19}F NMR spectra present an intense resonance due to the CF_3 groups of the ligand at -62.1 and -61.5 ppm for EuL^1 and EuL^2 , respectively, indicating the almost exclusive formation of SAP isomers (Figure S8, Supporting Information). In the case of EuL^2 a broad resonance at -62.7 ppm identifies the presence of a small fraction of TSAP isomer, with an abundance $< 10\%$. The presence of a single major ^{19}F NMR signal in EuL^1 implies a fast rotation on the NMR time scale about the NH-C bond of the phenyl group. The presence of a single ^{19}F NMR signal is important from the perspective of MRI to maximise the signal intensity provided by the probe.^[40]

The emission spectra recorded for the EuL^1 and EuL^2 complexes in H_2O present the typical $^5D_0 \rightarrow ^7F_J$ transitions of Eu^{3+} ($J = 0-4$, Figure S9, Supporting Information).^[41] The spectra present a single and well-defined $^5D_0 \rightarrow ^7F_0$ transition, which suggests the presence of a single species in solution. The splitting of the two components observed for the $^5D_0 \rightarrow ^7F_1$ transition (158 and 185 cm^{-1} for EuL^1 and EuL^2 , respectively), are characteristic of SAP isomers (i. e. 190 and 120 cm^{-1} for the SAP and TSAP isomers of EuDOTA^- , respectively).^[42]

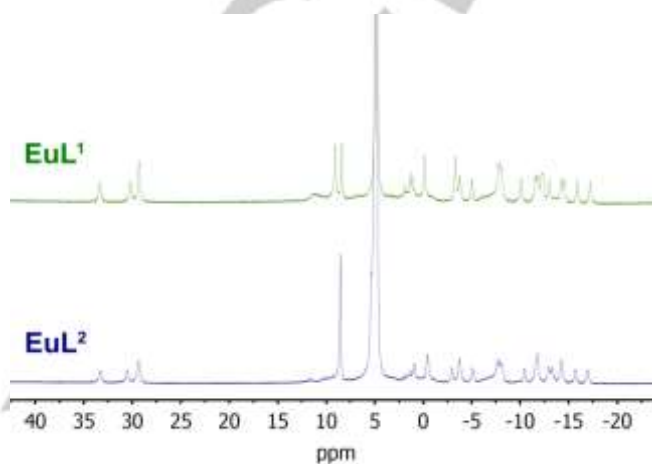


Figure 1. ^1H NMR spectra (D_2O , 300 MHz, 25 °C) of the EuL^1 and EuL^2 complexes (pH = 6.9 and 7.3, respectively).

The structure of the GdL^1 and GdL^2 complexes was also investigated by DFT calculations using well-established methods (see computational details below).^[43] These calculations provide the expected SAP and TSAP isomers as local energy minima. The relative Gibbs free energies obtained with DFT favour the SAP isomer by $\sim 1.9 \text{ kJ mol}^{-1}$ for both complexes, which is in perfect agreement with the spectroscopic data. The $\text{Gd-O}_{\text{water}}$ distance calculated for the SAP isomer of GdL^2 (2.428 Å) is shorter than that of GdL^1 (2.458 Å), which is a consequence of the positive charge of the complex. This anticipates a slower exchange rate of the coordinated water molecule in GdL^2 , as a stronger $\text{Gd-O}_{\text{water}}$ interaction implies a higher energy to reach the octacoordinated transition state following a dissociative mechanism.^[44]

^1H NMRD and ^{17}O NMR measurements. ^1H NMRD profiles were recorded to gain insight regarding the different physicochemical parameters that affect the observed relaxivity on both gadolinium complexes. The NMRD profiles were measured at 10, 25 and 37 °C in the 0.01 to 70 MHz proton Larmor frequencies range. All profiles present shapes that are typical of small and rapidly rotating Gd^{3+} complexes, which generally show a plateau at low fields ($< 1 \text{ MHz}$), a dispersion in the range 1-10 MHz, and a fairly constant relaxivity above 20 MHz.^[45] The relaxivities of GdL^1 decrease when the temperature is increased, and this effect is typical of complexes in which relaxivity is mainly limited by fast rotation. On the other hand, the relaxivity of GdL^2 remains nearly constant with temperature on

the range 10-37 °C, indicating that a low water exchange is limiting relaxivity, particularly at low temperatures.^[36,46] The relaxivities of the two complexes at 37 °C and 20 MHz are however very similar.

¹⁷O NMR transverse relaxation rates and chemical shifts were measured to obtain information of the exchange rate of the coordinated water molecule. The relaxation data obtained for GdL¹ present a maximum at ca. 52 °C that signals a changeover from the slow exchange regime at low temperatures to fast exchange at higher temperatures. For GdL² $1/T_2$ increases with temperature over the whole range, indicating a slower water exchange rate. The fit of the transverse relaxation and chemical shift data was performed using the Swift-Connick equations, following a well-established methodology.^[47] The scalar hyperfine coupling constants A/h obtained from the fits of the ¹⁷O NMR data fall within the typical range observed for Gd³⁺ complexes,^[43] confirming the reliability of the analysis. The water exchange rate determined for GdL¹ ($k_{ex}^{298} = 1.5 \times 10^6 \text{ s}^{-1}$) is somewhat lower than that reported for GdDOTA⁻.^[45a] This is attributed to: i) the almost exclusive presence of a SAP isomer in

solution in GdL¹, as SAP isomers present water exchange rates 40- 800-fold lower than TSAP ones;^[48-50] ii) The neutral charge of the GdL¹ complex compared to the negatively charged GdDOTA⁻, as increasing the positive charge of the complex generally results in lower water exchange rates.^[51] This effect is very evident when comparing the k_{ex}^{298} values of GdL¹ and GdL², as the two complexes are present in solution almost exclusively as SAP isomers.

The water exchange rate determined for GdL¹ is virtually identical to that reported for the SAP isomer of GdHPDO3A (Table 2, see also Scheme 3).^[49] Furthermore, the k_{ex}^{298} value obtained for GdL² matches very well that reported for the SAP isomer of [Gd(DOTA-2DMA)]⁺.^[50] The corresponding water exchange rates reported for the minor TSAP isomers present in solution are 112×10^6 and $70.4 \times 10^6 \text{ s}^{-1}$ for GdHPDO3A and [Gd(DOTA-2DMA)]⁺, respectively. These results confirm that the GdL¹ and GdL² complexes adopt SAP coordination environments, and that the charge of the complex plays a very important role in the water exchange of the coordinated water molecule.

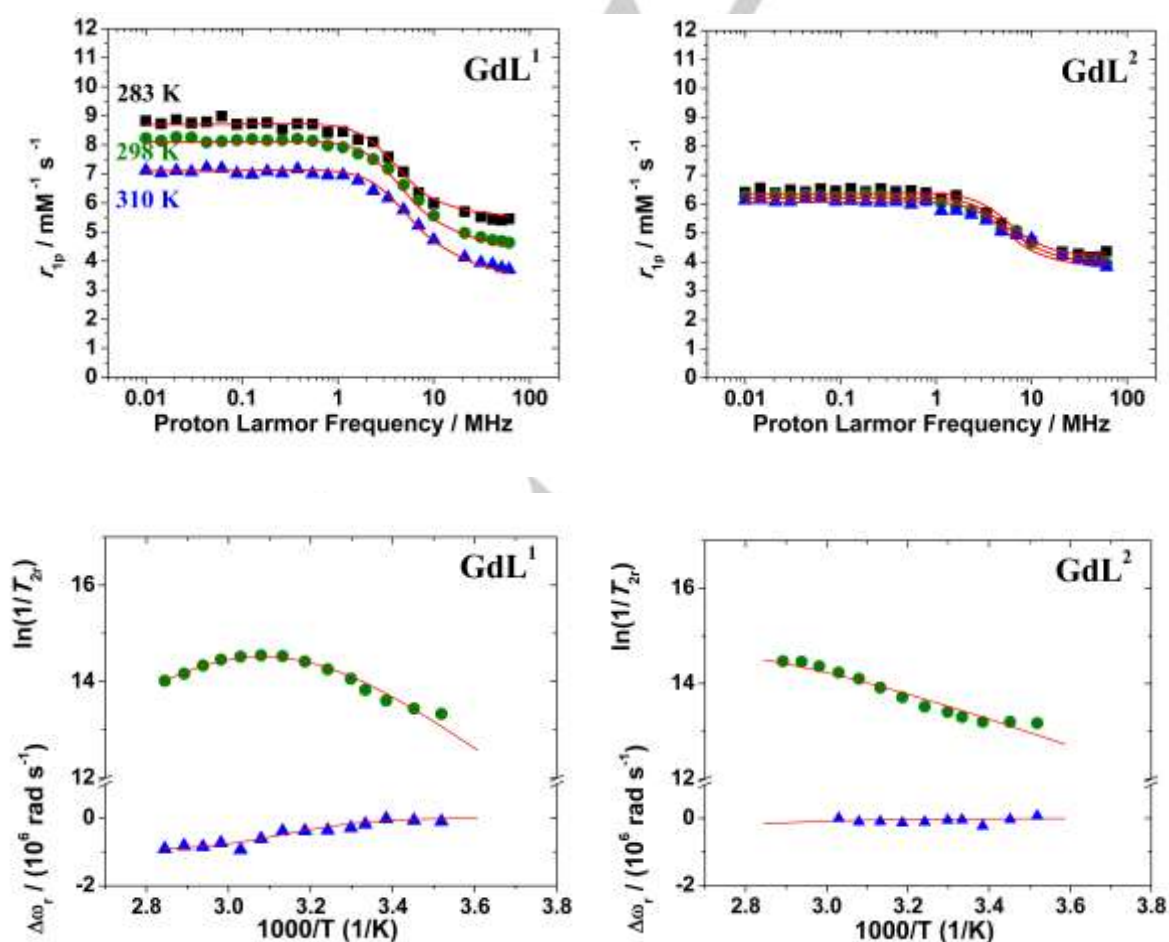
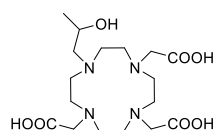
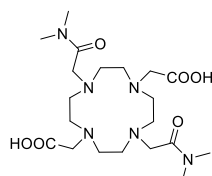


Figure 2. ¹H NMRD profiles at different temperatures (top) and ¹⁷O transverse relaxation rates and chemical shifts (bottom, 11.75 T) recorded for GdL¹ and GdL². The solid lines correspond to the fits of the data as described in the text.

Table 2. Parameters obtained from the analysis of the ^1H NMRD and ^{17}O NMR data.

[a]	GdL ¹	GdL ²	GdHPDO3A ^[b]	GdDOTA-2DMA ^[c]	GdDOTA ^[d]
r_{1p} (25/37 °C) / mM ⁻¹ s ⁻¹	4.97/4.14	4.26/4.23	4.8/3.7		4.2/3.6
k_{ex}^{298} / 10 ⁶ s ⁻¹	1.52 ± 0.17	0.73 ± 0.04	1.56	0.74	4.1
ΔH^\ddagger / kJ mol ⁻¹	49.6 ± 3.5	22.9 ± 2.0	53	50 ^[a]	49.8
τ_R^{298} / ps	98.3 ± 2.8	94.0 ± 2	65		77
E_r / kJ mol ⁻¹	15.6 ± 1.1	15.6 ^[a]			16.1
τ_V^{298} / ps	24.4 ± 2.0	15.4 ± 0.4	8	9.7	11
E_v / kJ mol ⁻¹	1.0 ^[a]	1.0 ^[a]			1.0 ^[a]
D_{GdH}^{298} / 10 ⁻¹⁰ m ² s ⁻¹	24.4 ± 0.1	24.4 ^[a]	22.2		22
E_{DGdH} / kJ mol ⁻¹	24.5 ± 3.5	15.3 ± 0.8			20.2
Δ^2 / 10 ¹⁹ s ⁻²	2.9 ± 0.3	7.4 ± 0.4	9.9	1.1	1.6
A_0/\hbar / 10 ⁷ rad s ⁻¹	-4.1 ± 0.3	-3.8 ± 0.3	-3.5		-3.7
$r_{GdH}/\text{\AA}$	3.1 ^[a]	3.1 ^[a]	3.0 ^[a]		3.1 ^[a]
$a_{GdH}/\text{\AA}$	4.0 ^[a]	4.0 ^[a]	3.8 ^[a]		3.5 ^[a]
q^{298}	1 ^[a]	1 ^[a]	1 ^[a]	1 ^[a]	1 ^[a]

[a] Parameters fixed during the fitting procedure. [b] Data for the SAP isomer from reference [49]. [c] Data obtained for the SAP isomer from reference [50]. [d] Data from reference [45a].

H₃HPDO3A**H₂DOTA-2DMA****Scheme 3.** Chemical structure of the ligands discussed in the text for comparative purposes.

The ^1H NMRD data was analysed using the standard Solomon-Bloembergen-Morgan theory for the inner-sphere contribution to relaxivity,^[52] and Freed's model to account for the outer-sphere contribution.^[53] The water exchange rates and their corresponding activation energies were set to the values obtained from ^{17}O NMR data. Following the standard procedure some of the parameters affecting relaxivity were fixed to typical values: the distance between the proton nuclei of the coordinated water molecule and the Gd^{3+} ion r_{GdH} was fixed to 3.1 Å,^[54] the number of coordinated water molecules q was set to one, the distance of closest approach of an outer-sphere water molecule was taken as $a_{\text{GdH}} = 4.0$ Å, and the activation energy for the modulation of the zero-field splitting was fixed at $E_v = 1$ kJ mol⁻¹. In the case of GdL² two additional parameters had to be fixed to obtain reasonable fitted parameters as a consequence of the negligible temperature dependence of r_{1p} : the diffusion coefficient D_{GdH}^{298} was fixed to 24.4×10^{-10} m² s⁻¹ and the activation energy for the rotational correlation time E_r was set to 15.6 kJ mol⁻¹. The rotational correlation times (τ_R^{298}) obtained from the fits of the data (~100 ps) are typical of small Gd^{3+} complexes. The same holds for the parameters describing the relaxation of the electron spin (the mean square zero-field-splitting energy, Δ^2 , and its correlation time τ_v), which take

values that are similar to those determined for Gd^{3+} complexes of DOTA derivatives (Table 2).

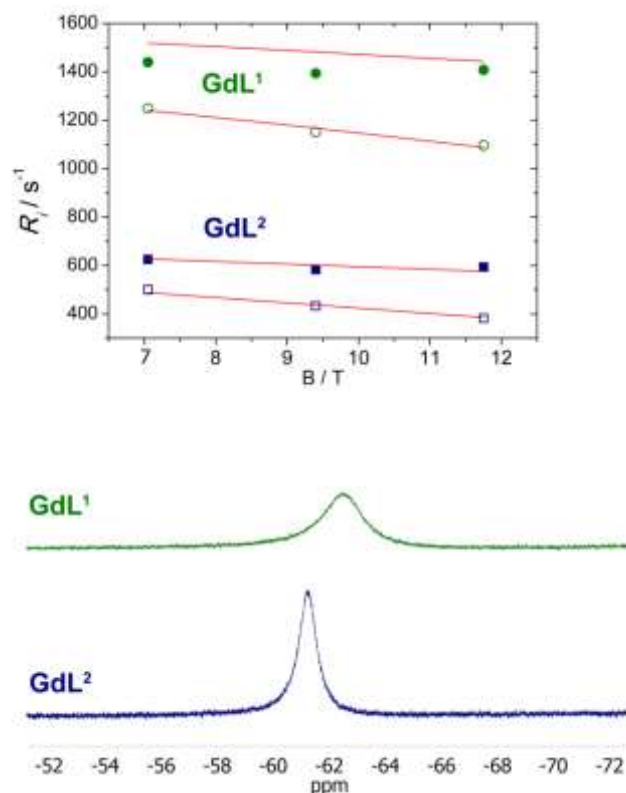
**Figure 3.** Top: longitudinal (R_1 , open symbols) and transverse (R_2 , closed symbols) relaxation rates recorded for GdL¹ and GdL². The solid lines correspond to the fits of the data as described in the text. Bottom: ^{19}F NMR spectra (7.05 T, 25 °C) of GdL¹ and GdL². All measurements were obtained using 5 mM concentrations based on Gd^{3+} .

Table 3. ^{19}F NMR longitudinal (T_1) and transverse (T_2) relaxation times obtained at different magnetic fields (25 °C).

	B [T]	T_1 [ms]	T_2 [ms]	T_2/T_1
GdL ¹	7.05	0.80	0.69	0.86
	9.4	0.87	0.71	0.82
	11.75	0.91	0.71	0.78
GdL ²	7.05	2.00	1.60	0.80
	9.4	2.31	1.71	0.74
	11.75	2.62	1.69	0.65

^{19}F measurements. The ^{19}F NMR spectra of GdL¹ and GdL² present a single broad resonance at 63.08 and 61.25 ppm, respectively (Figure 3). The signal is clearly broader for GdL¹ as compared to GdL². The longitudinal and transverse relaxation rates measured at 7.05, 9.4 and 11.75 T are in line with the trend observed for the linewidths, with GdL¹ being characterised by faster relaxation rates (Figure 3, Table 3). The ^{19}F relaxation rates of Gd³⁺ complexes are dominated by the dipolar contribution, as given by:^[55]

$$R_1 = \frac{2}{15} \frac{\gamma_I^2 g^2 \mu_B^2}{r_{\text{GdF}}^6} S(S+1) \left(\frac{\mu_0}{4\pi}\right)^2 \left[7 \frac{\tau_{C2}}{1+\omega_S^2 \tau_{C2}^2} + 3 \frac{\tau_{C1}}{1+\omega_I^2 \tau_{C1}^2} \right] \quad [1]$$

$$R_2 = \frac{1}{15} \frac{\gamma_I^2 g^2 \mu_B^2}{r_{\text{GdF}}^6} S(S+1) \left(\frac{\mu_0}{4\pi}\right)^2 \left[13 \frac{\tau_{C2}}{1+\omega_S^2 \tau_{C2}^2} + 3 \frac{\tau_{C1}}{1+\omega_I^2 \tau_{C1}^2} + 4\tau_{C1} \right] \quad [2]$$

In these equations S is the electron spin ($S = 7/2$ for Gd³⁺), γ_I is the nuclear gyromagnetic ratio, g is the electron g factor, μ_B is the Bohr magneton, r_{GdF} is the nuclear-spin-electron-spin distance and ω_I and ω_S are the nuclear and electron Larmor frequencies. τ_{C1} and τ_{C2} are given by:

$$\frac{1}{\tau_{Ci}} = \frac{1}{\tau_R} + \frac{1}{T_{ie}} \quad i = 1, 2 \quad [3]$$

At high magnetic fields $T_{ie} \gg \tau_R$, so that τ_R is the correlation time that dominates in Eq [3]. Thus, the ^{19}F relaxation data were fitted to Eqs [1] and [2], providing the

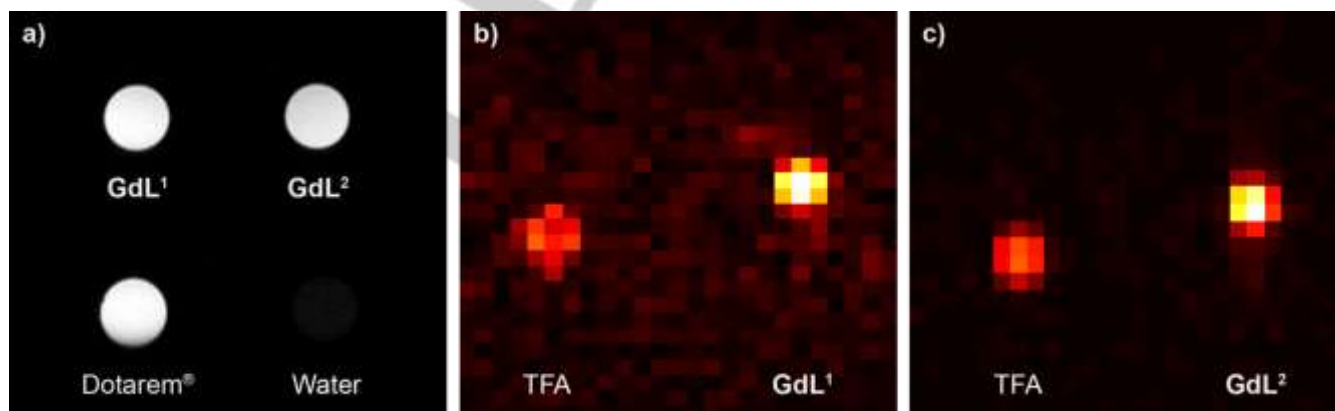
values of τ_R and r_{GdF} shown in Table 4. The longer rotational correlation time obtained for GdL² can be ascribed to the higher molecular weight of this complex compared to GdL¹. It is worth noting that the rotational correlation times shown in Table 4 correspond to the rotation of the Gd...F vector. Thus, it is not surprising that they are considerably longer than those obtained from ^1H NMRD data (Table 2), which correspond to the rotation of the Gd...H vector involving the proton nuclei of the coordinated water molecule. The local mobility of the coordinated water molecule is responsible for the shorter τ_R values evaluated from ^1H NMRD. Longer rotational correlation times were for instance obtained from ^{17}O NMR measurements for the Gd...O vector of coordinated water molecules, compared with those obtained with ^1H NMRD.^[56]

Table 4. Parameters obtained from the analysis of the ^{19}F NMR longitudinal and transverse relaxation data.

	τ_{RF} [ps]	r_{GdF} [Å] ^[a]	r_{GdF} [Å] ^[b]
GdL ¹	166 ± 19	7.4 ± 0.1	7.3
GdL ²	237 ± 16	9.1 ± 0.1	9.4

[a] Obtained from relaxation data. [b] Obtained from DFT calculations.

The r_{GdF} distance obtained from ^{19}F NMR data for GdL¹ (7.4 Å) is considerably shorter than that calculated for GdL² (9.1 Å), as would be expected considering the different position of the CF₃ groups on the phenyl ring(s) of the ligand. This relatively small distance variation (1.7 Å) causes an important effect on the observed R_1 and R_2 values, which is mainly related to the inverse sixth power relationship of r_{GdF} with R_1 and R_2 . The DFT structure described above for GdL² presents rather different r_{GdF} distances involving the CF₃ groups in *cis* (average at 6.83 Å) and *trans* (average at 9.75 Å) with respect to the amide oxygen atom. Thus, the r_{GdF} distance was estimated by averaging the $(1/r_{\text{GdF}})^6$ values obtained with DFT calculations, resulting in $r_{\text{GdF}} = 9.4$ Å. The dependence of both R_1 and R_2 on $(1/r_{\text{GdF}})^6$ implies that those F nuclei with shorter r_{GdF} distances provide a higher contribution to the observed relaxation rates. Following the same procedure, the DFT structure gives $r_{\text{GdF}} = 7.3$ Å for GdL¹. These values are in excellent agreement with those obtained from ^{19}F relaxation data, which confirms the reliability of the analysis.

**Figure 4.** ^1H and ^{19}F MRI on tube phantoms (5 mM complex, 7.05 T, RT). a) ^1H MRI of GdL¹⁻² along with those obtained for an equimolar amount of GdDOTA (Dotarem[®]) and pure water; b) ^{19}F MRI of GdL¹ and TFA (10 mM) and c) ^{19}F MRI of GdL² and TFA (10 mM).

^1H and ^{19}F MRI studies. The potential of GdL^{1-2} for their use as dual ^1H / ^{19}F MRI probes was assessed by means of MRI on tube phantoms at 7.05 T magnetic field, using 5 mM buffered solutions of the complexes (equivalent to 30 mM fluorine). For ^1H MRI, the phantom study consisted of GdL^1 , GdL^2 , GdDOTA^- (Dotarem[®]) and water, using the latter two samples as controls (Figure 4a). All Gd-containing samples had the same concentration of this paramagnetic ion (5 mM), resulting in comparable MR signal intensities upon performing the T_1 -weighted MRI. This result is indeed expected, given the similar r_{1p} values of GdL^{1-2} (see above) and GdDOTA^- .^[57]

For ^{19}F MRI, separate experiments were performed for GdL^1 and GdL^2 , respectively (Figure 4b,c). Namely, due to the difference in their ^{19}F T_1 and T_2 relaxation times (Table 3), optimization of ^{19}F MRI experimental parameters was performed first for achieving the maximal SNR to the given set of ^{19}F T_1 and T_2 (see ESI), and thus used different flip angles for the utilised fast low angle single shot (FLASH) pulse sequence. For comparison, in each experiment was used a tube with a solution of TFA (10 mM), which contained the same amount of fluorine as in the paramagnetic complex (30 mM). The resulting ^{19}F MR images indicated the affirmative properties of these complexes, especially GdL^2 . Namely, the obtained signal-to-noise ratio (SNR) for GdL^2 after 1 hour acquisition time was 103, which was over 50% higher than that of TFA (67). Concurrently, a lower SNR was observed in the experiment with GdL^1 , again being doubled relative to TFA (SNR = 22 and 11 for GdL^1 and TFA, respectively). If the SNR=2 is taken as the border-line detection limit of the measurement, we estimate detection limits of ~450 and ~100 μM for GdL^1 and GdL^2 , respectively. These estimates suggest an improvement in sensitivity of the measurement with almost twice lower GdL^2 concentration needed for detection compared to the previously reported Gd^{3+} complex containing a fluorinated aryl-phosphonate group.^[58] On one hand, both GdL^1 and GdL^2 show that PRE effect of Gd^{3+} reduces the ^{19}F relaxation times to significant extent, thus resulting in greater SNR values in ^{19}F MRI experiments for paramagnetic probes relative to diamagnetic samples (TFA). On the other hand, different structural properties of GdL^1 and GdL^2 are clearly reflected on the final ^{19}F MRI results as well. One should note that a shorter Gd...F distance in GdL^1 results in much stronger PRE effect and thus shorter ^{19}F T_1 and T_2 relaxation times, with T_2 being over 6 times shorter in GdL^1 than in GdL^2 (Table 3). Consequently, such dramatic shortening of T_2 leads to substantial loss of signal in the ^{19}F MRI experiments of GdL^1 relative to GdL^2 . For GdL^2 , the PRE effect of the adjacent Gd^{3+} also shortens both ^{19}F T_1 and T_2 ; however, the slightly longer Gd...F distance this time provides an affirmative T_2/T_1 ratio, which is reflected in ^{19}F MR images with very high SNR. Indeed, considering the obtained SNR values, one could significantly reduce the acquisition times for GdL^2 to the level of 5-10 min, still expecting the SNR>10 in the analogous ^{19}F MRI experiment.

Conclusions

Two cyclen-based Gd^{3+} complexes were designed and synthesised as potential dual $^1\text{H}/^{19}\text{F}$ MRI contrast agents. The presence of a coordinated water molecule yields ^1H relaxivities comparable to those of the commercially available contrast agent GdDOTA^- (Dotarem[®]), though the slower water exchange in the bis-amide derivative results in a somewhat lower relaxivity. An interesting feature of these complexes is their presence in solution as a single major species, which was characterised as the square antiprismatic (SAP) isomer. The shorter Gd...F distance determined for GdL^1 (7.4 Å) results in considerably shorter T_1 and T_2 relaxation times compared with GdL^2 (Gd...F = 9.1 Å). Phantom studies evidenced that the slightly longer transverse relaxation of GdL^2 yields good SNRs compared to GdL^1 . Thus, a Gd...F distance in the range 9-10 Å appears to be optimal for the design of efficient Gd^{3+} -based MRI probes. The study reported here paves the way for the preparation of genuine $^1\text{H}/^{19}\text{F}$ MRI probes characterised by high stability and inertness.

Experimental Section

Materials and methods.

$\text{DO3A}^t\text{Bu}$ and $\text{DO2A}^t\text{Bu}$ were purchased from CheMatech (Dijon, France). All other reagents and solvents were commercial and used without further purification. ^1H , ^{19}F and ^{13}C NMR spectra were recorded on Bruker Avance 300 MHz, Bruker Avance III HD 400 MHz and Bruker Avance 500 MHz spectrometers.

High-resolution electrospray-ionization time-of-flight ESI-TOF mass spectra were recorded using a LC-Q-q-TOF Applied Biosystems QSTAR Elite spectrometer in positive and negative mode. Elemental analyses were accomplished on a ThermoQuest Flash EA 1112 elemental analyser. Medium performance liquid chromatography (MPLC) was carried out using a Puriflash XS 420 instrument equipped with a reverse-phase Puriflash 15C18HP column (60 Å, spherical 15 μm , 20 g) and UV-DAD detection at 210 and 254 nm, and operating at a flow rate of 10 mL/min. Aqueous solutions were lyophilised using a Telstar Cryodos-80 apparatus.

2-chloro-N-(3,5-di-trifluoromethyl-phenyl)acetamide (1a): A solution of chloroacetyl chloride (11.5 mmol) in acetic acid (5 mL) was added dropwise to a mixture of 3,5-bis(trifluoromethyl)aniline (9.78 mmol) in acetic acid (35 mL) at 0 °C. The reaction mixture was maintained at room temperature for an additional 4 hours. Subsequently it was slowly poured into 100 mL of ice water. The aqueous solution was extracted with CH_2Cl_2 (4x100 mL). The combined organic phase was dried over anhydrous Na_2SO_4 , filtered and the solvent was evaporated to furnish a solid residue. Yield: 92%. ^1H -NMR (solvent CDCl_3 , 298 K, 400 MHz) δ_{H} (ppm): 8.52 (s, 1H, NH), 8.07 (s, 2H, CH_{Ph}), 7.67 (s, 1H, CH_{Ph}), 4.23 (s, 2H, CH_2). ^{13}C -NMR (solvent CDCl_3 , 298 K, 101 MHz) δ_{C} (ppm): 164.4, (quaternary, CO), 138.1 (quaternary, C_{Ph}), 133.1-132.1 (quaternary, CF_3), 127.0 (tertiary, CH_{Ph}), 124.3 (tertiary, CH_{Ph}), 121.6 (quaternary, CH_{Ph}), 119.9, 118.9, 118.6, 118.6, 118.6, 42.7 (secondary, CH_2). ^{19}F -

NMR (solvent CDCl₃, 298 K, 376 MHz) δ_F (ppm): -63.09. Mass spectrometry (ESI⁻) m/z (%BPI): 304.00 (100) ([C₁₀H₅ClF₆NO]⁻); 339.98 (7) (C₁₀H₆ClF₆NO[Cl]⁻). HR-MS (ESI⁻) m/z : [M]⁻, calculated: 303.9958, found: 303.9959.

2-chloro-N-(4-(trifluoromethyl)phenyl)acetamide (1b): Chloroacetyl chloride (12.0 mmol) in dry CH₂Cl₂ (20 mL) was slowly added dropwise to a mixture of 4-(trifluoromethyl)aniline (10.0 mmol) and NaHCO₃ (25.5 mmol) in dry CH₂Cl₂ (30 mL) at 0 °C. The reaction mixture was stirred at 0 °C for an additional 4 hours. At a subsequent stage it was slowly poured into 80 mL of water. The aqueous solution was extracted with CH₂Cl₂ (8x150 mL). The combined organic layer was washed with brine and dried over anhydrous Na₂SO₄. The solvent was evaporated to dryness to afford a solid residue. Yield: 97%. ¹H-NMR (solvent CDCl₃, 298 K, 300 MHz) δ_H (ppm): 8.35 (s, 1H, NH), 7.71-7.61 (dd, 4H, CH_{Ph}), 4.22 (s, 2H, CH₂). ¹³C-NMR (solvent CDCl₃, 298 K, 75 MHz) δ_C (ppm): 164.0 (quaternary, CO), 139.8 (quaternary, C_{Ph}), 126.4 (tertiary, C_{Ph}), 126.4 (tertiary, CH_{Ph}), 119.7 (quaternary, CH_{Ph}), 42.8 (secondary, CH₂). ¹⁹F-NMR (solvent CDCl₃, 298 K, 282 MHz) δ_F (ppm): -62.26. Mass spectrometry (ESI⁻) m/z (%BPI): 236.02 (100) ([C₉H₆ClF₃NO]⁻); 272.00 (6) (C₉H₇ClF₃NO[Cl]⁻). HR-MS (ESI⁻) m/z : [M]⁻, calculated: 236.0095, found: 236.0099.

General procedure for the preparation of the ligands: The cyclen derivative was dissolved in CH₃CN (25 mL) under basic conditions. A solution of the corresponding 2-chloro-N-substituted-acetamide in CH₃CN (20 mL) was added dropwise to the mixture at ambient temperature. The reaction was heated at 45 °C for several days, until the alkylation was completed. The reaction mixture was removed from heat and allowed to cool to room temperature, filtered and reduced to dryness *in vacuo*. The yellow oil was redissolved in CH₂Cl₂ and washed with water. The organic layer was concentrated under vacuum pressure to afford a yellowish oil. The product was purified by neutral alumina chromatography, eluting with CHCl₃ in gradient up to 5% in MeOH to yield a yellowish foam. Final ligands H₃L¹ and H₂L² were achieved by deprotection of the *tert*-butyl groups with formic acid (5 mL), stirred at reflux for 48 h. Subsequently, the acid was removed and the residue was washed several times with water (5x10 mL). The product was redissolved in water and lyophilised to achieve a yellowish solid.

1,4,7-Tris(tert-butoxycarbonylmethyl)-10-((3,5-(trifluoromethyl)phenyl)acetamide)-1,4,7,10-tetraazacyclododecane (2a). DO3A*t*Bu (0.526 g, 1.02 mmol), 2-chloro-N-(3,5-(trifluoromethyl)phenyl)acetamide (0.360 g, 1.175 mmol, 1.15 equiv), K₂CO₃ (0.353 g, 2.55 mmol, 2.5 equiv), stirred at 45 °C during 9 days. Yellow foam (0.645 g, 81%). ¹H-NMR (300 MHz, CDCl₃) δ_H (ppm): 12.12 (s, 1H, NH), 8.36 (s, 2H, CH_{Ph}), 7.45 (s, 1H, CH_{Ph}), 3.80 (s, 2H, CH₂), 3.51-1.92 (m, 22H, CH₂), 1.61 (s, 9H, CH₃), 1.46-1.37 (s, 18H, CH₃). ¹³C-NMR (solvent CDCl₃, 298 K, 75 MHz) δ_C (ppm): 172.6 (quaternary, CO), 172.3 (quaternary, CO), 151.9 (quaternary, CO), 140.8 (quaternary, CH_{Ph}), 131.5 (tertiary, CH_{Ph}), 120.5 (quaternary, CF₃), 116.2 (tertiary, CH_{Ph}), 116.1 (tertiary, CH_{Ph}), 82.4 (quaternary, CCH₃), 56.8 (secondary, CH₂), 55.8 (secondary, CH₂), 55.5 (secondary, CH₂), 29.7 (secondary, CH₂), 27.9 (primary, CH₂), 27.8 (primary, CH₂). ¹⁹F-NMR (solvent CDCl₃, 298 K, 282 MHz) δ_F (ppm): -63.05. Mass spectrometry (ESI⁺) m/z (%BPI): 806.39 (100) ([C₃₆H₅₅F₆N₅NaO₇]⁺); 784.41 (2) ([C₃₆H₅₆F₆N₅O₇]⁺).

Triacetic 1,4,7-Tris(carboxymethyl)-10-((3,5-(trifluoromethyl)phenyl)acetamide)-1,4,7,10-tetraazacyclododecane acid (H₃L¹). Brownish solid (0.5060 g, quantitative). ¹H-NMR (300 MHz, D₂O): δ_H (ppm): 8.36 (s, 1H, CH_{Ph}), 8.06 (s, 2H, CH_{Ph}), 7.84 (s, 1H, NH), 3.89-3.16 (m, 24H, CH₂). ¹³C-NMR (solvent D₂O, 298 K, 75 MHz) δ_C (ppm): 174.3 (quaternary, CO), 172.6 (quaternary, CO), 140.0 (quaternary, HN-C_{Ph}), 133.7-132.8 (quaternary, CF₃), 128.2 (quaternary, C_{Ph}), 126.6 (tertiary, CH_{Ph}), 123.0 (quaternary, CF₃), 120.2 (tertiary,

CH_{Ph}), 59.1 (secondary, CCH₃), 54.5 (secondary, CH₂), 52.5 (secondary, CH₂), 51.9 (secondary, CH₂), 31.9 (primary, CH₂). ¹⁹F-NMR (solvent D₂O, 298 K, 282 MHz) δ_F (ppm): -62.66. Mass spectrometry (ESI⁺) m/z (%BPI): 638.20 (96) ([C₂₄H₃₁F₆N₅NaO₇]⁺); 676.15 (63) ([C₂₄H₃₀F₆KN₅NaO₇]⁺), 698.13 (100) ([C₂₄H₂₉F₆KN₅Na₂O₇]⁺); 714.11 (67) ([C₂₄H₂₉F₆K₂N₅NaO₇]⁺). HR-MS (ESI⁺) m/z : [M+Na]⁺, calculated: 638.2019, found: 638.2014.

1,7-bis(tert-butoxycarbonylmethyl)-4,10-((4-(trifluoromethyl)phenyl)acetamide)-1,4,7,10-tetraazacyclododecane (2b). Cyclen derivative DO2A*t*Bu (0.117 g, 0.2928 mmol), 2-chloro-N-(4-(trifluoromethyl)phenyl)acetamide (0.165 g, 0.6978 mmol, 2.4 equiv), K₂CO₃ (0.2014 g, 5 equiv). The reaction was heated to reflux for 9 days. Yellow crude solid (0.235 g, quantitative). ¹H NMR (300 MHz, CDCl₃) δ_H (ppm): 9.73 (s, 2H, NH), 7.86-7.84 (d, 4H, CH_{Ph}), 7.32-7.30 (d, 4H, CH_{Ph}), 3.47-2.07 (m, 22H, CH₂), 1.32 (s, 9H, CH₃), 1.27 (s, 9H, CH₃). ¹³C-NMR (solvent CDCl₃, 298 K, 75 MHz) δ_C (ppm): 171.6 (quaternary, CO), 170.8 (quaternary, CO), 141.6 (quaternary, C_{Ph}), 129.5 (tertiary, CH_{Ph}), 125.9-124.6 (quaternary, CF₃), 122.3 (tertiary, CH_{Ph}), 119.7 (secondary, CH₂), 119.3 (secondary, CH₂), 118.7 (secondary, CH₂), 116.5 (secondary, CH₂), 81.8 (quaternary, CCH₃), 81.5 (quaternary, CCH₃), 58.7 (secondary, CH₂), 58.4 (secondary, CH₂), 57.2 (secondary, CH₂), 56.6 (secondary, CH₂), 52.1 (secondary, CH₂), 27.9 (primary, CH₂). ¹⁹F-NMR (solvent CDCl₃, 298 K, 282 MHz) δ_F (ppm): -62.33. Mass spectrometry (ESI⁺) m/z (%BPI): 825.38 (100) ([C₃₈H₅₂F₆N₆NaO₆]⁺); 803.40 (2) ([C₃₈H₅₃F₆N₆O₆]⁺).

Diacetic 1,7-Bis(carboxymethyl)-10-((4-(trifluoromethyl)phenyl)acetamide)-1,4,7,10-tetraazacyclododecane acid (H₂L²). Light yellow solid (0.202 g, quantitative). ¹H NMR (300 MHz, D₂O): δ_H (ppm): 8.42 (s, 2H, CH_{Ph}), 7.66 (s, 2H, NH), 7.41 (s, 6H, CH_{Ph}), 3.53-2.89 (m, 24H, CH₂). ¹³C-NMR (solvent D₂O, 298 K, 101 MHz) δ_C (ppm): 172.1 (quaternary, CO), 171.0 (quaternary, CO), 140.1 (quaternary, C_{Ph}), 125.9 (tertiary, CH_{Ph}), 125.4 (quaternary, CF₃), 120.9 (tertiary, CH_{Ph}), 57.2 (quaternary, CCH₃), 55.1 (secondary, CH₂), 51.9 (secondary, CH₂), 50.4 (secondary, CH₂). ¹⁹F-NMR (solvent D₂O, 298 K, 282 MHz) δ_F (ppm): -62.05. Mass spectrometry (ESI⁺) m/z (%BPI): 713.25 (100) ([C₃₀H₃₆F₆N₆NaO₆]⁺); 751.20 (40) ([C₃₀H₃₅F₆KN₆NaO₆]⁺), 729.22 (25) ([C₃₀H₃₆F₆KN₆O₆]⁺), 691.27 (17) ([C₃₀H₃₇F₆N₆O₆]⁺). HR-MS (ESI⁺) m/z : [M+Na]⁺, calculated: 713.2492, found: 713.2503.

General procedure for the preparation of the complexes: The corresponding ligand H₃L¹ or H₂L² was solved in *n*-butanol in the presence of base (DIPEA) and the solution was homogenised with ultrasound bath assistance. The corresponding hydrated LnCl₃ (Ln = Eu, Gd or Tb) were added in solid state to the mixture and heated at 112 °C for 6 h. Subsequently the mixture was allowed to cool down and the solvent was removed by the use of the rotary evaporator to achieve an orange crude. The reaction mixture was purified by reverse-phase medium performance liquid chromatography (MPLC). For the neutral complexes, the purification method was carried out in gradient of solvent B (CH₃CN, 10 to 30%) in solvent A (H₂O). For the charged complexes, the purification was performed in gradient of solvent B (0.01% Et₃N in CH₃CN, 5 to 15%) in solvent A (0.01% Et₃N in H₂O). The fractions containing the complexes were combined and the solvent was removed *in vacuo*. The final product was redissolved in water and lyophilised to furnish the final complexes.

EuL¹. White solid (0.0309 g, 64%). Mass spectrometry (ESI⁺) m/z (%BPI): 788.10 (100) ([C₂₄H₂₈N₅O₇F₆NaEu]⁺). HR-MS (ESI⁺) m/z : [M+Na]⁺, calculated: 788.0997, found: 788.0994.

GdL¹. White solid (0.0282 g, 56%). Mass spectrometry (ESI⁺) m/z (%BPI): 793.10 (100) ([C₂₄H₂₈N₅O₇F₆NaGd]⁺). HR-MS (ESI⁺) m/z : [M+Na]⁺, calculated: 793.1026, found: 793.0992.

TbL¹. White solid (0.0479 g, 54%). Mass spectrometry (ESI⁺) m/z (%BPI): 794.10 (100) ([C₂₄H₂₈N₅O₇F₆NaTb]⁺). HR-MS (ESI⁺) m/z: [M+Na]⁺, calculated: 794.1038, found: 794.1045.

EuL². White solid (0.0291 g, 31%). Mass spectrometry (ESI⁺) m/z (%BPI): 841.17 (100) ([C₃₀H₃₄N₆O₆F₆Eu]⁺). HR-MS (ESI⁺) m/z: [M]⁺, calculated: 841.1650, found: 841.1651.

GdL². White solid (0.0286 g, 31%). Mass spectrometry (ESI⁺) m/z (%BPI): 846.17 (100) ([C₃₀H₃₄N₆O₆F₆Gd]⁺). HR-MS (ESI⁺) m/z: [M]⁺, calculated: 846.1679, found: 846.1673.

TbL². White solid (0.0517 g, 56%). Mass spectrometry (ESI⁺) m/z (%BPI): 847.17 (100) ([C₃₀H₃₄N₆O₆F₆Tb]⁺). HR-MS (ESI⁺) m/z: [M]⁺, calculated: 847.1692, found: 847.1698.

Relaxometric measurements: Relaxivities of the Gd³⁺ complexes were measured at 298 K and 300 MHz using a Bruker Advance III 300 MHz spectrometer and aqueous solutions buffered at pH 7.4 (0.05 M HEPES) containing 10% D₂O for locking purposes. Proton NMRD profiles were measured at 10, 25 and 37 °C over a continuum of magnetic fields from 0.0002 to 0.25 T (corresponding to 0.01-10 MHz proton Larmor frequencies) on a fast field-cycling Stelar SmarTracer relaxometer (Mede, Pv, Italy). The relaxometer operates under computer control with an absolute uncertainty in 1/T₁ of ± 1%. The temperature control was carried out using a Stelar VTC-91 airflow heater equipped with a calibrated copper–constantan thermocouple (uncertainty of ± 0.1 K). Data points at higher field strengths were measured on a Stelar Spinmaster relaxometer in the range from 0.5 to 1.5 T (20-60 MHz proton Larmor frequencies) equipped with a Bruker WP80 electromagnet adapted to variable-field measurements. A Bruker Advance III spectrometer (11.75 T) equipped with a 5 mm probe and standard temperature control unit was used to perform ¹⁷O NMR measurements. Samples in aqueous solution used for the measurements contained 2.0% of the ¹⁷O isotope (Cambridge Isotope). The observed transverse relaxation rates were established from the signal width at half-height. The exact concentrations of all solutions used for ¹H relaxivity and ¹⁷O NMR measurements were determined by the bulk magnetic susceptibility (BMS) method.^[59]

Computational details: All the calculations were carried out by using the Gaussian 09 package (Revision E.01).^[60] Full-geometry optimizations of the [GdL¹] and [GdL²]⁺ complexes were performed in aqueous solution by employing DFT within the hybrid meta-generalised gradient approximation (hybrid meta-GGA) with the TPSSh exchange-correlation functional.^[61] The large-core quasi-relativistic effective core potential (LCRECP) developed by Dolg and co-workers and the associated [5s4p3d]-GTO valence-basis set was employed for the lanthanides,^[62] whereas the ligand atoms were described by using the standard 6–31G(d,p) basis set. The stationary points found on the potential-energy surfaces as a result of geometry optimizations were tested to represent energy minima rather than saddle points by using frequency analysis. Solvent effects were included by using the integral-equation formalism variant of the polarizable continuum model (IEFPCM).^[63]

Magnetic resonance imaging. MRI measurements on tube phantoms were performed on Bruker BioSpec 70/30 USR magnet (software version Paravision 5.1) using a Bruker volume coil (RF RES 300 1H 075/040 QSN TR). ¹H and ¹⁹F MR images were acquired using Fast Low Angle Single Shot (FLASH) pulse sequence. ¹H phantom consisted of 4 x 400 μL vials containing 5 mM of GdL¹, GdL², GdDOTA⁻ (Dotarem[®]) and water. ¹⁹F phantom consisted of a pair of such vials containing either 5 mM of GdL¹ or GdL² with equimolar concentration of TFA (calculated per fluorine atoms) as a reference.

¹H MR image was acquired using following parameters: field of view (FOV) = 31.8 x 31.8 mm², matrix size (MTX) = 212 x 212, slice thickness 0.5 mm, flip angle (FA) = 90°, repetition time (TR) = 10 ms, echo time (TE) = 2.746 ms, number of excitations (NEX) = 10, and total acquisition time (TA) = 21.2 sec. ¹⁹F MR imaging parameters were: FOV = 32 x 32, MTX = 32 x 32, slice thickness 5 mm, FA = 89° (GdL¹)/ 78° (GdL²), TR = 3.2 ms, TE = 1.01 ms, NEX = 35156, TA = 60 min. The imaging parameters TR and FA were optimised using Eq. [4].^[64]

$$\text{SNR} = \frac{\left(\frac{\sin(\text{FA}) \left(1 - \exp\left(-\frac{\text{TR}}{T_1}\right) \right)}{1 - \exp\left(-\frac{\text{TR}}{T_1} \cos(\text{FA})\right)} \right)}{\sqrt{\text{TR}}} \quad [4]$$

Acknowledgements

Authors R. P.-P., D. E.-G. and C. P.-I. thank Ministerio de Economía y Competitividad (CTQ2016-76756-P) and Xunta de Galicia (ED431B 2017/59 and ED431D 2017/01) for generous financial support and Centro de Supercomputación de Galicia (CESGA) for providing the computer facilities. R. P.-P. thanks Ministerio de Economía y Competitividad for a PhD FPI grant (BES-2014-068399) and fellowships for short term stays in Tübingen (EEBB-I-17-12213) and Alessandria (EEBB-I-18-13075). M.B. is grateful to Università del Piemonte Orientale for financial support (Ricerca locale 2016). T.S. thanks the German Academic Exchange Service (DAAD) for the Ph.D. fellowship. This work was carried out within the framework of the COST CA15209 Action “European Network on NMR Relaxometry”.

Keywords: Gadolinium • MRI • Macrocycles • NMR spectroscopy • Fluorine

- [1] B.-T. Doan, S. Meme, J.-C. Beloeil in *The Chemistry of Contrast Agents in Medical Magnetic Resonance Imaging*, (Eds.: A. Merbach, L. Helm, E. Toth), John Wiley & Sons, Chichester, **2013**, pp. 1-23.
- [2] J. Wahsner, E. M. Gale, A. Rodriguez-Rodriguez, P. Caravan, *Chem. Rev.* **2019**, DOI: 10.1021/acs.chemrev.8b00363.
- [3] S. Faulkner, O. A. Blackburn, in *The Chemistry of Molecular Imaging*, (Eds.: N. Long, W.-T. Wong), John Wiley & Sons, Hoboken, **2015**, pp. 179-197.
- [4] L. M. De León-Rodríguez, A. F. Martins, M. C. Pinho, N. M. Rofsky, A. D. Sherry, *J. Magn. Reson. Imaging* **2015**, *42*, 545-565.
- [5] H. U. Rashid, M. A. U. Martines, J. Jorge, P. M. de Moraes, M. N. Umar, K. Khan, H. U. Rehman, *Bioorg. Med. Chem.* **2016**, *24*, 5663-5684.
- [6] a) M. Rogosnitzky, S. Branch, *Biometals* **2016**, *29*, 365-376. b) L. Caschera, A. Lazzara, L. Piergallini, D. Ricci, B. Tuscano, A. Vanzulli, *Pharmacol. Res.* **2016**, *110*, 65-75.
- [7] I. A. Dekkers, R. Roos, A. J. van der Molen, *Eur. Radiol.* **2018**, *28*, 1579-1584.
- [8] Z. Baranyai, Z. Palinkas, F. Uggeri, A. Maiocchi, S. Aime, E. Brücher, *Chem. Eur. J.* **2012**, *18*, 16426-16435.
- [9] J. R. Morrow, E. Toth, *Inorg. Chem.* **2017**, *56*, 6029-6034.
- [10] a) B. Drahos, I. Lukes, E. Toth, *Eur. J. Inorg. Chem.* **2012**, 1975-1987. b) M. Kueny-Stotz, A. Garofalo and D. Felder-Flesch, *Eur. J. Inorg. Chem.* **2012**, 1987-2005. c) G. S. Loving, S. Mukherjee and P. Caravan, *J. Am. Chem. Soc.*, **2013**, *135*, 4620-4623. d) E. M. Gale, S. Mukherjee, C. Liu, G. S. Loving and P. Caravan, *Inorg. Chem.*, **2014**, *53*, 10748-10761. e) M. Regueiro-Figueroa, G. A. Rolla, D. Esteban-

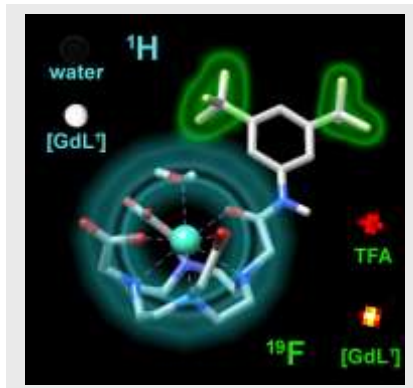
- Gomez, A. de Blas, T. Rodriguez-Blas, M. Botta, C. Platas-Iglesias, *Chem. Eur. J.* **2014**, *20*, 17300-17305.
- [11] N. Kuznik, M. Wyskocka, *Eur. J. Inorg. Chem.* **2016**, 445-458.
- [12] a) S. J. Dorazio, P. B. Tsitovich, K. E. Sifers, J. A. Sperryak, J. R. Morrow, *J. Am. Chem. Soc.* **2011**, *133*, 14154-14156. b) P. B. Tsitovich, J. M. Cox, J. A. Sperryak, J. R. Morrow, *Inorg. Chem.* **2016**, *55*, 12001-12010. c) S. J. Dorazio, J. R. Morrow, *Inorg. Chem.* **2012**, *51*, 7448-7450. d) S. J. Dorazio, J. R. Morrow, *Eur. J. Inorg. Chem.* **2012**, 2006-2014.
- [13] a) P. B. Tsitovich, J. A. Sperryak, J. R. Morrow, *Angew. Chem. Int. Ed.* **2013**, *52*, 13997-14000. b) S. J. Dorazio, A. Olatunde, J. A. Sperryak, J. R. Morrow, *Chem. Commun.* **2013**, *49*, 10025-10027. c) A. E. Thorarinnsson, K. Du, J. H. P. Collins, T. D. Harris, *J. Am. Chem. Soc.* **2017**, *139*, 15836-15847.
- [14] a) A. Olatunde, S. J. Dorazio, J. A. Sperryak, J. R. Morrow, *J. Am. Chem. Soc.* **2012**, *134*, 18503-18505. b) L. Caneda-Martínez, L. Valencia, I. Fernandez-Perez, M. Regueiro-Figueroa, G. Angelovski, I. Brandariz, D. Esteban-Gomez and C. Platas-Iglesias, *Dalton Trans.* **2017**, *46*, 15095-15106.
- [15] a) S. J. Dorazio, A. O. Olatunde, P. B. Tsitovich, J. R. Morrow, *J. Biol. Inorg. Chem.* **2014**, *19*, 191-205. b) A. Olatunde, C. J. Bond, S. Dorazio, J. M. Cox, J. B. Benedict, M. D. Daddario, J. A. Sperryak, J. R. Morrow, *Chem. Eur. J.* **2015**, *21*, 18290-18300.
- [16] a) S. Viswanathan, Z. Kovacs, K. N. Green, S. J. Ratnakar, A. D. Sherry *Chem. Rev.* **2010**, *110*, 2960-3018. b) E. Terreno, D. D. Castelli, S. Aime, *Contrast Media Mol. Imaging* **2010**, *5*, 78-98.
- [17] a) P. Harvey, A. M. Blamire, J. I. Wilson, K.-L. N. A. Finney, A. M. Funk, P. K. Senanayake, D. Parker, *Chem. Sci.* **2013**, *4*, 4251-4258. b) P. B. Tsitovich, J. M. Cox, J. B. Benedict, J. R. Morrow, *Inorg. Chem.* **2016**, *55*, 700-716.
- [18] a) G. Angelovski, *Acc. Chem. Res.* **2017**, *50*, 2215-2224. b) G. Angelovski, É. Tóth, *Chem. Soc. Rev.*, **2017**, *46*, 324-336.
- [19] a) M. C. Heffern, L. M. Matosziuk, T. J. Meade, *Chem. Rev.* **2014**, *114*, 4496-4539. b) J. L. Major, T. J. Meade, *Acc. Chem. Res.* **2009**, *42*, 893-903.
- [20] a) S. N. M. Chilla, C. Henoumont, L. Vander Elst, R. N. Muller, S. Laurent, *Isr. J. Chem.* **2017**, *57*, 800-808. b) E. Debroye, T. N. Parac-Vogt, *Chem. Soc. Rev.* **2014**, *43*, 8178-8192.
- [21] J. Ruiz-Cabello, B. P. Barnett, P. A. Bottomley, J. W. Bulte, *NMR Biomed.* **2011**, *24*, 114-119.
- [22] J.-X. Yu, R. R. Hallac, S. Chiguru, R. P. Mason, *Progress in Nuclear Magnetic Resonance Spectroscopy* **2013**, *70*, 25-49.
- [23] K. L. Peterson, K. Srivastava, V. C. Pierre, *Front. Chem.* **2018**, 6:160.
- [24] J. Blahut, P. Hermann, A. Gálisová, V. Herynek, I. Cisařová, Z. Tošnerc, J. Kotek, *Dalton Trans.*, **2016**, *45*, 474-478.
- [25] a) M. Yu, D. Xie, K. P. Phan, J. S. Enriquez, J. J. Luci, E. L. Que, *Chem. Commun.* **2016**, *52*, 13885-13888. b) J. Blahut, K. Bernásek, A. Galisova, V. Herynek, I. Cisarova, J. Kotek, J. Lang, S. Matejkova, P. Hermann, *Inorg. Chem.* **2017**, *56*, 13337-13348.
- [26] K. H. Chalmers, E. De Luca, N. H. M. Hogg, A. M. Kenwright, I. Kuprov, D. Parker, M. Botta, J. I. Wilson, A. M. Blamire, *Chem. Eur. J.*, **2010**, *16*, 134-148.
- [27] a) K. H. Chalmers, M. Botta, D. Parker, *Dalton Trans.* **2011**, *40*, 904-913. b) K. H. Chalmers, A. M. Kenwright, D. Parker, A. M. Blamire, *Magn. Reson. Med.*, **2011**, *66*, 931-936. c) P. Harvey, I. Kuprov, D. Parker, *Eur. J. Inorg. Chem.* **2012**, 2015-2022. d) P. K. Senanayake, A. M. Kenwright, D. Parker, S. K. van der Hoorn, *Chem. Commun.*, **2007**, 2923-2925. e) A. M. Kenwright, I. Kuprov, E. De Luca, D. Parker, S. U. Pandya, P. K. Senanayake, D. G. Smith, *Chem. Commun.*, **2008**, 2514-2516.
- [28] a) K. Srivastava, E. A. Weitz, K. L. Peterson, M. Marjanska, V. C. Pierre, *Inorg. Chem.* **2017**, *56*, 1546-1557. b) K. Srivastava, G. Ferrauto, V. G. Young, Jr., S. Aime, V. C. Pierre, *Inorg. Chem.* **2017**, *56*, 12206-12213.
- [29] a) P. Kadjane, C. Platas-Iglesias, P. Boehm-Sturm, V. Truffault, G. E. Hagberg, M. Hoehn, N. K. Logothetis, G. Angelovski, *Chem. Eur. J.* **2014**, *20*, 7351-7362. b) N. Cakic, T. Savic, J. Stricker-Shaver, V. Truffault, C. Platas-Iglesias, C. Mirkes, R. Pohmann, K. Scheffler, G. Angelovski, *Chem. Commun.* **2016**, *52*, 9224-9227. c) N. Cakić, B. Tickner, M. Zaiss, D. Esteban-Gómez, C. Platas-Iglesias, G. Angelovski, *Inorg. Chem.* **2017**, *56*, 14, 7737-7745.
- [30] A. Keliris, K. Scheffler, J. Engelmann in *Fluorine Magnetic Resonance Imaging*, (Eds.: U. Flögel, E. Ahrens), Pan Stanford Publishing Pte. Ltd., Singapore, **2013**, pp. 141-170.
- [31] A. J. Pella, G. Pintacuda, C. P. Grey, *Paramagnetic NMR in solution and the solid state, Progress in Nuclear Magnetic Resonance Spectroscopy* **2018**, 1-825.
- [32] Q. Ji, D. Yang, X. Wang, C. Chen, Q. Deng, Z. Ge, L. Yuan, X. Yang, F. Liao, *Bioorg. Med. Chem.*, **2014**, *22*, 3405-3413.
- [33] Z. Xiaohe, Q. Yu, Y. Hong, S. Xiuqing, Z. Rugang, *Chem. Biol. Drug Des.* **2010**, *76*, 330-339.
- [34] A. Rodriguez-Rodriguez, D. Esteban-Gomez, R. Tripiet, G. Tircso, Z. Garda, I. Toth, A. de Blas, T. Rodriguez-Blas, C. Platas-Iglesias, *J. Am. Chem. Soc.* **2014**, *136*, 17954-17957.
- [34] L. Helm in *Contrast Agents for MRI. Experimental Methods* (Eds.: V. C. Pierre, M. J. Allen), The Royal Society of Chemistry, Croydon, **2018**, p. 122.
- [36] A. L. Thompson, D. Parker, D. A. Fulton, J. A. K. Howard, S. U. Pandya, H. Puschmann, K. Senanayake, P. A. Stenson, A. Badari, M. Botta, S. Avedano, S. Aime, *Dalton Trans.* **2006**, *0*, 5605-5616.
- [37] A. Beeby, I. M. Clarkson, R. S. Dickins, S. Faulkner, D. Parker, L. Royle, A. S. de Sousa, J. A. G. Williams, M. Woods, *J. Chem. Soc. Perkin Trans. 2* **1999**, 493-503.
- [38] a) R. M. Supkowski, W. DeW. Horrocks, Jr., *Inorg. Chim. Acta* **2002**, *340*, 44-48. b) M. Woods, S. Aime, M. Botta, J. A. K. Howard, J. M. Moloney, M. Navet, D. Parker, M. Port, O. Rousseaux, *J. Am. Chem. Soc.* **2000**, *122*, 9781-9792.
- [39] a) C. Kumas, W. S. Fernando, P. Zhao, M. Regueiro-Figueroa, G. E. Kiefer, A. F. Martins, C. Platas-Iglesias, A. D. Sherry, *Inorg. Chem.* **2016**, *55*, 9297-9305. b) C. Adair, M. Woods, P. Y. Zhao, A. Pasha, P. M. Winters, G. M. Lanza, P. Athey, A. D. Sherry, G. E. Kiefer, *Contrast Media Mol. Imaging* **2007**, *2*, 55-58. c) M. Polasek, J. Kotek, P. Hermann, I. Cisarova, K. Binnemans, I. Lukes, *Inorg. Chem.* **2009**, *48*, 466-475. d) F. A. Dunand, R. S. Dickins, D. Parker, A. E. Merbach, *Chem. Eur. J.* **2001**, *7*, 5160-5167.
- [40] E. De Luca, P. Harvey, K. H. Chalmers, A. Mishra, P. K. Senanayake, J. I. Wilson, M. Botta, M. Fekete, A. M. Blamire, D. Parker, *J. Biol. Inorg. Chem.*, **2014**, *19*, 215-227.
- [41] K. Binnemans, *Coord. Chem. Rev.* **2015**, *295*, 1-45.
- [42] R. S. Dickins, D. Parker, J. I. Bruce, D. J. Tozer, *Dalton Trans.* **2003**, 1264-1271.
- [43] D. Esteban-Gomez, A. de Blas, T. Rodriguez-Blas, L. Helm, C. Platas-Iglesias, *ChemPhysChem* **2012**, *13*, 3640-3650.
- [44] M. Regueiro-Figueroa, C. Platas-Iglesias, *J. Phys. Chem. A* **2015**, *119*, 6436-6445.
- [45] a) D. H. Powell, O. M. Ni Dhubghaill, D. Pubanz, L. Helm, Y. S. Lebedev, W. Schlaepfer, A. E. Merbach, *J. Am. Chem. Soc.* **1996**, *118*, 9333-9346. b) H. Lammers, F. Maton, D. Pubanz, M. W. van Laren, H. van Bekkum, A. E. Merbach, R. N. Muller, J. A. Peters, *Inorg. Chem.* **1997**, *36*, 2527-2538.
- [46] a) G. M. Nicolle, F. Yerly, D. Imbert, U. Bottger, J.-C. G. Bünzli, A. E. Merbach, *Chem. Eur. J.* **2003**, *9*, 5453-5467. b) S. Aime, M. Botta, M. Fasano, *Chem Eur J* **1997**, *3*, 1499-1504.
- [47] a) T. J. Swift, R. E. Connick, *J. Chem. Phys.* **1962**, *37*, 307-320. b) T. J. Swift, R. E. Connick, *J. Chem. Phys.* **1964**, *41*, 2553-2554.
- [48] a) F. A. Dunand, R. S. Dickins, D. Parker, A. E. Merbach, *Chem. Eur. J.* **2001**, *7*, 5160-5167. b) F. A. Dunand, S. Aime, A. E. Merbach, *J. Am. Chem. Soc.* **2000**, *122*, 1506-1512.
- [49] D. Delli Castelli, M. C. Caligara, M. Botta, E. Terreno, S. Aime, *Inorg. Chem.* **2013**, *52*, 7130-7138.
- [50] S. Zhang, Z. Kovacs, S. Burgess, S. Aime, E. Terreno, A. D. Sherry, *Chem. Eur. J.* **2001**, *7*, 288-296.

- [51] J. Henig, E. Toth, J. Engelmann, S. Gottschalk, H. A. Mayer, *Inorg. Chem.* **2010**, *49*, 6124-6138.
- [52] a) I. Solomon, *Phys. Rev.* **1955**, *99*, 559-565. b) I. Solomon, N. Bloembergen, *J. Chem. Phys.* **1956**, *25*, 261-266. c) N. Bloembergen, *J. Chem. Phys.* **1957**, *27*, 572-573. d) N. Bloembergen, L. O. Morgan, *J. Chem. Phys.* **1961**, *34*, 842-850.
- [53] J. H. Freed, *J. Chem. Phys.* **1978**, *68*, 4034-4037.
- [54] A. V. Astashkin, A. M. Raitsimring, P. Caravan, *J. Phys. Chem. A* **2004**, *108*, 1990-2001.
- [55] J. A. Peters, J. Huskens, D. J. Raber, *Prog. Nucl. Magn. Reson. Spectrosc.* **1996**, *28*, 283-350.
- [56] F. A. Dunand, A. Borel, A. E. Merbach, *J. Am. Chem. Soc.* **2002**, *124*, 710-716.
- [57] J. B. Livramento, C. Weidensteiner, M. I. M. Prata, P. R. Allegrini, C. Geraldes, L. Helm, R. Kneuer, A. E. Merbach, A. C. Santos, P. Schmidt, É. Toth, *Contrast Media Mol. Imaging* **2006**, *1*, 30-39.
- [58] M. P. Placidi, M. Botta, F. K. Kalman, G. E. Hagberg, Z. Baranyai, A. Krenzer, A. K. Rogerson, I. Toth, N. K. Logothetis, G. Angelovski, *Chem. Eur. J.* **2013**, *19*, 11644-11660.
- [59] D. M. Corsi, C. Platas-Iglesias, H. van Bekkum, J. A. Peters, *Magn. Reson. Chem.* **2001**, *39*, 723-726.
- [60] M. J. Frisch, G. W. Trucks, H. B. Schlegel, G. E. Scuseria, M. A. Robb, J. R. Cheeseman, G. Scalmani, V. Barone, B. Mennucci, G. A. Petersson, H. Nakatsuji, M. Caricato, X. Li, H. P. Hratchian, A. F. Izmaylov, J. Bloino, G. Zheng, J. L. Sonnenberg, M. Hada, M. Ehara, K. Toyota, R. Fukuda, J. Hasegawa, M. Ishida, T. Nakajima, Y. Honda, O. Kitao, H. Nakai, T. Vreven, J. A. Montgomery Jr., J. E. Peralta, F. Ogliaro, M. Bearpark, J. J. Heyd, E. Brothers, K. N. Kudin, V. N. Staroverov, R. Kobayashi, J. Normand, K. Raghavachari, A. Rendell, J. C. Burant, S. S. Iyengar, J. Tomasi, M. Cossi, N. Rega, N. J. Millam, M. Klene, J. E. Knox, J. B. Cross, V. Bakken, C. Adamo, J. Jaramillo, R. Gomperts, R. E. Stratmann, O. Yazyev, A. J. Austin, R. Cammi, C. Pomelli, J. W. Ochterski, R. L. Martin, K. Morokuma, V. G. Zakrzewski, G. A. Voth, P. Salvador, J. J. Dannenberg, S. Dapprich, A. D. Daniels, O. Farkas, J. B. Foresman, J. V. Ortiz, J. Cioslowski, D. J. Fox in *Gaussian 09, Revision A.01*; Gaussian, Inc., Wallingford, CT, **2009**.
- [61] J. M. Tao, J. P. Perdew, V. N. Staroverov, G. E. Scuseria, *Phys. Rev. Lett.* **2003**, *91*, 146401-146404.
- [62] M. Dolg, H. Stoll, A. Savin, H. Preuss, *Theor. Chim. Acta* **1989**, *75*, 173-194.
- [63] J. Tomasi, B. Mennucci, R. Cammi, *Chem. Rev.* **2005**, *105*, 2999-3093.
- [64] M. A. Bernstein, K. F. King, X. J. Zhou in *Handbook of MRI Pulse Sequences*, Elsevier Academic Press, Burlington, MA; London, **2004**, p. 1017.

Entry for the Table of Contents

FULL PAPER

Gadolinium(III) complexes containing cyclen units, functionalized with pendant arms that incorporate $-\text{CF}_3$ substituents, provide response in Magnetic Resonance Imaging at both the ^1H and ^{19}F frequencies.



Rosa Pujales-Paradela, Tanja Savić, David Esteban-Gómez, Goran Angelovski,* Fabio Carniato, Mauro Botta,* Carlos Platas-Iglesias[†]

Page No. – Page No.

Gadolinium(III)-based Dual $^1\text{H}/^{19}\text{F}$ MRI Probes